Theoretical study of asymmetric molecular-frame photoelectron angular distributions for C 1s photoejection from CO_2

S. Miyabe,[1,2] C. W. McCurdy,[1,2,3] A. E. Orel,[3] and T. N. Rescigno[1]

[1]*Chemical Sciences, Lawrence Berkeley National Laboratory, Berkeley, California 94720, USA*
[2]*Department of Chemistry, University of California, Davis, California 95616, USA*
[3]*Department of Applied Science, University of California, Davis, California 95616, USA*

We report the results of *ab initio* calculations of cross sections and molecular-frame photoelectron angular distributions for C 1s ionization of CO_2 and propose a mechanism for the recently observed asymmetry of those angular distributions with respect to the CO^+ and O^+ ions produced by subsequent Auger decay. The fixed-nuclei, photoionization amplitudes were constructed using variationally obtained electron-molecular ion scattering wave functions. We have also carried out electronic structure calculations which identify a dissociative state of the CO_2^{2+} dication that is likely populated following Auger decay and which leads to $O^+ + CO^+$ fragment ions. We show that a proper accounting of vibrational motion in the computation of the photoelectron angular distributions, along with reasonable assumptions about the nuclear dissociation dynamics, gives results in good agreement with recent experimental observations. We also demonstrate that destructive interference between different partial waves accounts for sudden changes with photon energy in the observed angular distributions.

I. INTRODUCTION

Coincident measurement of *K*-shell photoelectrons and fragment ion momenta from molecular dissociation following Auger decay allows one to study photoelectron angular distributions in the molecular frame (MFPAD) [1]. These distributions are generally far richer than conventionally measured laboratory-frame angular distributions, which are typically characterized by a single asymmetry parameter. A good example is afforded by the recent experiments and accompanying theoretical calculations on C 1s ionization from CO_2 reported by Saito *et al.* [2] and Liu *et al.* [3] These experiments showed several striking features. The body-frame photoelectron angular distributions for photon polarization along the molecular axis were found to be characterized by simple two-lobed patterns, in good agreement with the reported calculations, except over a narrow range of photon energies where there were marked deviations from these simple patterns and where theory and experiment showed marked differences. The experiments also showed a weak but definite asymmetry in the photoelectron angular distributions with respect to the $O^+ + CO^+$ fragment ions, which is surprising since the photoelectron is being ejected from the central carbon atom in this linear, symmetric molecule [3]. Liu *et al.* [3] speculated that this asymmetry might be due to an interference between gerade and ungerade intermediate states, resulting in a partial breakdown of the two-step model for core-level photoionization and subsequent Auger decay.

Our purpose here is to show that a proper accounting of vibrational motion in the target molecule, along with reasonable assumptions about the dissociation dynamics following Auger decay, can account for the observed angular distributions without invoking a breakdown of the two-step model. Analysis of the calculated results also shows that the rapid change in the photoelectron angular distributions over a narrow range of photon energies are due to interference effects between different partial-wave amplitudes.

The outline of this paper is as follows. In the following section, we describe the physical processes associated with C(1s) photoionization and our proposed mechanism for explaining the origin of asymmetric photoelectron angular distributions. Section III describes the theory and computational methods used. We begin with a description of the electron structure calculations we carried out on the final CO_2^{2+} dication states. We then outline the methods used to compute MFPADs, including the treatment of vibrational motion. Our results are presented in Sec. IV. We conclude with a brief discussion.

II. MECHANISM FOR ASYMMETRIC MOLECULAR-FRAME PHOTOELECTRON ANGULAR DISTRIBUTIONS

Before describing the details of our theoretical calculations, we will begin with a physical description of the process of core-level photoionization, followed by Auger decay, and propose a mechanism that can explain how asymmetric angular distributions can arise when electrons are ejected from the central atom of a symmetric linear molecule. We will then go on to describe the theoretical calculations we performed that support our proposed mechanism.

In contrast to the valence electrons that are delocalized over the target nuclei, the central atom core-level electrons in CO_2 are tightly confined about the carbon atom. Absorption of an x-ray photon with energy >297.6 eV [4] results in the ejection of a carbon 1s electron. The interaction potential experienced by the ejected photoelectron as it exits the target molecule is determined by the target electron charge distribution, which is in turn sensitive to the instantaneous positions of the nuclei at the moment the photon is absorbed. The nuclei, on a time scale determined by the fundamental frequencies of the molecule, vibrate about their equilibrium positions. For the asymmetric-stretch mode, whose frequency is ~ 2349 cm^{-1}, the time scale for one complete vibration is
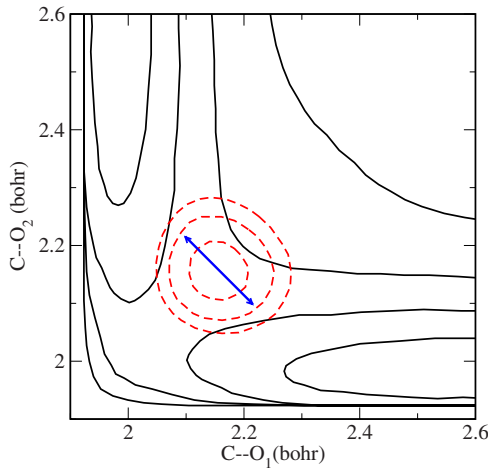
FIG. 1. (Color online) Contour plot of linear CO_2 ground-state potential surface from Ref. [5] (broken lines) superimposed on a repulsive CO_2^{2+} dication surface (solid lines). Double ended indicates asymmetric-stretch normal coordinate.

approximately 14.2 fs. To estimate the photoelectron angular distribution produced by photons absorbed at some particular asymmetric geometry, we can calculate the fixed-nuclei photoionization cross section at that geometry and multiply it by the square of the corresponding vibrational wave function, which gives the probability distribution for finding the nuclei at that position. Asymmetry in the fixed-nuclei cross section for certain geometries, however, is not sufficient to produce an observable effect since the asymmetry vanishes when it is averaged over an ensemble of molecules. What is further needed is another measurable process which can be recorded in coincidence with the photoelectron ejection and which retains the memory of any initial asymmetry in the target. Asymmetric ion fragmentation can, in principle, provide such a tool.

The core-hole state produced by photoionization is not stable and promptly (in ∼6 fs [6]) decays by Auger emission to produce a CO_2^{2+} dication. We assume that the decay takes place before the molecular ion can execute enough vibrational motion that would erase the memory of the geometry at which it was created. Auger decay can generally leave the dication in any number of electronic states, although there is a strong propensity for formation of singlet states in cases such as the present where the initial neutral molecule is a closed-shell singlet [7]. If there is a dissociative dication state(s) that leads *directly* to $O^+ + CO^+$ fragments, then any initial asymmetry in the CO bond lengths at the time the photon is absorbed will be reflected in the dissociation products, provided that the dissociative states (or state) are created by the Auger process before significant vibrational or rotational motion can occur. For the MFPAD to be measurable in these experiments, the axial recoil approximation must be valid for the dissociation of the dication. The combination of a directly dissociative state or states of CO_2^{2+} with the absence of significant rotational motion are both necessary to ensure that this is the case. (The neutral and dication potential surfaces in linear O-C-O geometry relevant to this discussion are sketched in Fig. 1.) Coincident measurement of photoelectrons and fragment ion momenta can then lead to

the observation of asymmetric angular distributions. So to summarize, the proposed mechanism requires:

(1) the fixed-nuclei carbon *K*-shell photoionization cross section to show a measurable asymmetry at geometries sampled by asymmetric-stretch vibrational motion;

(2) Auger decay to be fast enough that the molecule, in its transient $1s$ core-hole state, does not undergo enough vibrational motion to erase the memory of the geometry at which it was created;

(3) and a singlet electronic state of CO_2^{2+} that dissociates directly and promptly to $O^+ + CO^+$ fragments.

We will turn below to a description of the theoretical calculations we carried out that support these assumptions.

III. THEORY AND COMPUTATION

A. Electronic structure calculations

Hochlaf *et al.* [5] mapped the collinear paths along the OC-O coordinate for the low-lying electronic states of CO_2^{2+}, using a complete active space self-consistent field (CASSCF) approach. All of the singlet states they studied, with vertical excitation energies less than ∼8 eV relative to the ground $X\,^3\Sigma_g^-$ state of the dication, are separated by relatively large barriers from their dissociation asymptotes and thus present no viable candidates for the dissociative state we seek. The results of Hochlaf *et al.* [5] are consistent with the recently published study of the C $1s^{-1}$ Auger spectrum of CO_2 by Püttner *et al.* [8]. The latter authors reported that the lowest dissociative band in the Auger spectrum is centered near 10 eV, with a low-energy tail that overlaps an intense, narrow feature near 7.6 eV. The latter feature was attributed to an excited $^1\Sigma_g^+$ state, which had been identified in an earlier theoretical study by Feyer *et al.* [9] Püttner *et al.* [8] mentioned four excited states as possible candidates for the dissociative band, based largely on an early theoretical study of Ägren [10], but none of these states have been characterized in any detail.

The electronic structure calculations for this study were carried out using a multireference configuration-interaction approach. We employed Dunning's double-zeta plus polarization basis of contracted Gaussian functions for carbon and oxygen [11], augmented with two additional *p*-type functions on each atom. The calculations were carried out in linear geometry for the OC-O coordinate, with one CO distance fixed at the equilibrium geometry of the neutral molecule (2.20 bohr). The molecular orbitals were obtained from a CASSCF calculation on the $^3\Sigma_g^-$ ground state of the dication, and the configuration-interaction calculations on the singlet dication states included all single excitations relative to the complete active space, with the restriction that the carbon and oxygen $1s$ orbitals were kept doubly occupied. This procedure generated ∼1.2×10^6 configurations. The resulting OC-O potential energy curves are shown in Fig. 2 for the lowest singlet, $a\,^1\Delta$, the excited $2\,^1\Sigma^+$ state, confirming the assignment of Püttner *et al.* [8], and the three lowest $^1\Pi$ states. The two lowest $^1\Pi$ states agree reasonably well with the results of Hochlaf *et al.* [5]. We note that the geometry of the $2\,^1\Sigma^+$ state, whose dominant configuration is $3\sigma_u^{-2}$ at its minimum, is very close to that of the neutral molecule,
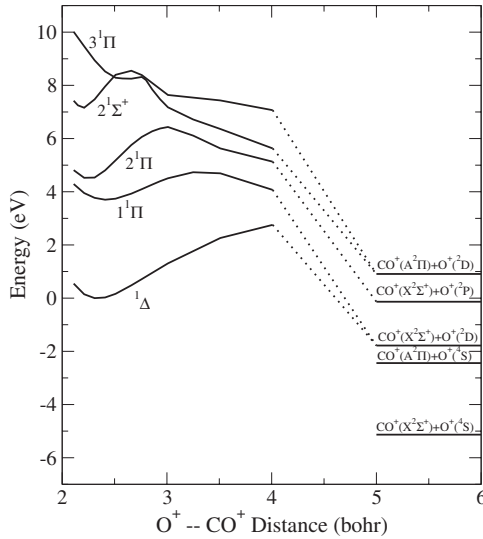
FIG. 2. Collinear potential energy curves for several low-lying singlet states of CO_2^{2+}. One CO distance is fixed at 2.20 bohr.

which explains why it gives rise to a sharp peak in the Auger spectrum. The $3\,^1\Pi$ state is dominated by the configuration $3\sigma_u^{-1}1\pi_u^{-1}$, $^1\Pi_g$ at small C-O distances, and correlates with excited CO^+ and O^+ fragments. In contrast to the other excited singlet states, it is the only state we found that, starting from the equilibrium geometry of the parent neutral, is not separated by a large barrier to dissociation into $O^+ + CO^+$ products. The $3\,^1\Pi$ state thus provides a direct path to asymmetric dissociation.

B. Computation of molecular-frame photoionization cross sections using the complex Kohn method

Fixed-nuclei photoionization amplitudes were computed using the complex Kohn variational method [12]. Since the method does not rely on single-center expansion to compute the required electron-molecular ion continuum wave functions, it is well suited to applications involving polyatomic targets. The application of the Kohn method to molecular photoionization has been previously described [13], so we will limit ourselves here to a brief summary.

The final-state wave function for production of photoions in a specific state Γ_0 is written as

$$\Psi_{\Gamma_0}^- = \sum_\Gamma A(\chi_\Gamma F_{\Gamma\Gamma_0}^-) + \sum_i d_i^{\Gamma_0}\Theta_i \tag{1}$$

where Γ labels the final ionic target states χ_Γ included, $F_{\Gamma\Gamma_0}^-$ are channel functions that describe the photoionized electron, A is the antisymmetrization operator, and the Θ_i's are N electron correlation terms. Note that we are using Γ_0 as a combined index to denote the target ion electronic state and the angular momentum quantum numbers l_0, m_0 of the ejected photoelectron. In the present application, only one ionic target state is included in the trial wave function—that being the $C(1s^{-1})$ hole state.

In the Kohn method, the channel functions are further expanded, in the molecular frame, as

$$F_{\Gamma\Gamma_0}^-(\mathbf{r}) = \sum_i c_i^{\Gamma\Gamma_0}\varphi_i(\mathbf{r}) + \sum_{lm}[f_{lm}(k_\Gamma,r)\delta_{ll_0}\delta_{mm_0}\delta_{\Gamma\Gamma_0}$$
$$+ T_{ll_0mm_0}^{\Gamma\Gamma_0}h_{lm}^-(k_\Gamma,r)]Y_{lm}(\hat{\mathbf{r}})/k_\Gamma^{1/2}r, \tag{2}$$

where the $\varphi_i(\mathbf{r})$ are a set of square-integrable (Cartesian Gaussian) functions and the $f_{lm}(k_\Gamma,\mathbf{r})$ and $h_{lm}^-(k_\Gamma,\mathbf{r})$ are numerical continuum functions that behave asymptotically as regular and incoming partial-wave Coulomb functions, respectively [14].

Photoionization cross sections in the molecular frame can be constructed from the matrix elements as follows:

$$I_{\Gamma_0}^\mu = \langle\Psi_{\Gamma_0}^-|r^\mu|\Psi_0\rangle, \tag{3}$$

where r^μ is a component of the dipole operator, which we evaluate here in the length form,

$$r^\mu = \begin{cases} z, & \mu = 0 \\ \mp(x \pm iy)/\sqrt{2}, & \mu = \pm 1 \end{cases} \tag{4}$$

and Ψ_0 is the initial state wave function of the neutral N electron target. In order to construct an amplitude that represents a photoelectron with momentum $\mathbf{k}_{\Gamma_0}$ ejected by absorption of a photon with polarization direction $\hat{\epsilon}$, measured relative to the molecular body frame, the matrix elements $I_{\Gamma_0}^\mu$ must be combined in a partial-wave series as follows:

$$I_{\mathbf{k}_{\Gamma_0},\hat{\epsilon}} = \sqrt{\frac{4\pi}{3}}\sum_{\mu l_0 m_0}i^{-l_0}e^{i\delta_{l_0}}I_{\Gamma_0}^\mu Y_{1\mu}(\hat{\epsilon})Y_{l_0 m_0}(\hat{k}_{\Gamma_0}), \tag{5}$$

where δ_{l_0} is a Coulomb phase shift. The cross section, differential in the angle of photoejection and photon polarization relative to the fixed body frame of the molecule, is then given (in atomic units) by

$$\frac{d^2\sigma}{d\Omega_{\hat{k}_{\Gamma_0}}d\Omega_{\hat{\epsilon}}} = \frac{8\pi\omega}{3c}|I_{\mathbf{k}_{\Gamma_0},\hat{\epsilon}}|^2, \tag{6}$$

where ω is the photon energy and c is the speed of light.

There is a technical note that we would like to mention before concluding this section [13]. The initial state Ψ_0 and final continuum state $\Psi_{\Gamma_0}^-$ should be orthogonal since they are formally solutions of the same N electron Hamiltonian. In practice, we use different approximations in computing these wave functions. This is not an issue for molecules with a center of symmetry, such as CO_2 in its equilibrium geometry, since dipole selection rules then require Ψ_0 and $\Psi_{\Gamma_0}^-$ to have opposite parities, which guarantees their orthogonality. In an asymmetric geometry, however, Ψ_0 and $\Psi_{\Gamma_0}^-$ are generally not orthogonal, which means that the transition dipole matrix elements can be contaminated by introducing a component of the static dipole moment of the target. We remedy this by explicitly orthogonalizing $\Psi_{\Gamma_0}^-$ to Ψ_0, i.e., by using the modified matrix elements,

$$\tilde{I}_{\Gamma_0}^\mu \equiv I_{\Gamma_0}^\mu - \langle\Psi_0|\mu|\Psi_0\rangle\langle\Psi_{\Gamma_0}^-|\Psi_0\rangle \tag{7}$$

to compute the photoionization amplitudes.

For practical reasons, the bound initial state and final combined state of the photoelectron and the ion must be

constructed using a common set of orthogonal orbitals. For a closed-shell target such as CO_2, it is reasonable to use a single-configuration space self-consistent field (SCF) wave function for the initial state. Using the same occupied molecular orbitals to construct the final ionic state, with a single vacancy in the carbon $1s$ orbital, simplifies the computation of the photoionization amplitude but ignores orbital relaxation effects caused by creation of the core vacancy. In the theoretical treatment reported by Saito *et al.* [2] and by Liu *et al.* [3] this problem was addressed by constructing a relaxed basis of molecular orbitals obtained by creating a fractional electron vacancy in the carbon K shell and then using those orbitals to construct both the neutral target and the ionic final state [15]. In our calculations, we will investigate the use of both neutral and ion orbitals, using natural orbital techniques to obtain the latter.

C. Inclusion of vibrational motion

Molecular photoionization cross sections are frequently calculated with the target nuclei fixed at their equilibrium positions. Such cross sections correspond, in cases where the internal motion of the target can be ignored, to vibrationally (and rotationally) summed quantities. To account for the target vibrational motion, which can account for asymmetry in the photoelectron angular distributions and which will turn out to be essential in comparing calculated and experimentally measured quantities, we make the Born-Oppenheimer approximation for the initial state and the final scattering states, writing them as products of electronic functions times vibrational functions (we can safely ignore rotation in the present context). We can then rewrite the amplitude [defined in Eq. (5)] for a particular $\nu \rightarrow \nu'$ transition as

$$I_{\mathbf{k}_{\Gamma_0},\hat{\epsilon}}^{\nu,\nu'} = \sqrt{\frac{4\pi}{3}} \sum_{\mu l_0 m_0} i^{-l_0} e^{i\delta_{l_0}} Y_{1\mu}(\hat{\epsilon}) Y_{l_0 m_0}(\hat{k}_{\Gamma_0})$$
$$\times \int I_{\Gamma_0}^{\mu}(\mathbf{s})\, \eta_\nu(\mathbf{s})\, \eta_{\nu'}(\mathbf{s})\, d\mathbf{s}, \tag{8}$$

where we have used $\mathbf{s}$ to denote the internal coordinates and η_ν and $\eta_{\nu'}$ are the initial (neutral) and final (ion) vibrational wave functions, respectively. Note that we have ignored the dependence of the photoelectron wave vector $\mathbf{k}_{\Gamma_0}$ on the final vibrational state, which is a good approximation except when very close to thresholds. If we are not interested in the excitation of individual vibrational levels, then we can sum over final ν' in computing the body-frame cross section, using the closure relation,

$$\sum_{\nu'} \eta_{\nu'}(\mathbf{s})\, \eta_{\nu'}(\mathbf{s}') = \delta(\mathbf{s} - \mathbf{s}'), \tag{9}$$

to obtain the differential body-frame photoionization cross section for a target molecule in initial vibrational state ν as follows:

$$\frac{d^2\sigma_\nu}{d\Omega_{\hat{k}_{\Gamma_0}} d\Omega_{\hat{\epsilon}}} = \int \eta_\nu(\mathbf{s})^2 \frac{d^2\sigma}{d\Omega_{\hat{k}_{\Gamma_0}} d\Omega_{\hat{\epsilon}}}(\mathbf{s})\, d\mathbf{s}. \tag{10}$$

We thus arrive at the intuitive result that the physical cross section is obtained by integrating the fixed-nuclei cross section over all internal geometries, with each geometry weighted by the square of the initial vibrational wave function, which is the probability of finding the target nuclei at a given geometry.

We approximate the initial vibrational wave function as a product of harmonic oscillator functions in the symmetric-stretch, asymmetric-stretch, and bending normal coordinates using force constants derived from our SCF calculations. We found that averaging over symmetric-stretch motion had little effect on the angular distributions, so the results we present include only asymmetric stretch and bending. Bending motion does not of course break the left/right symmetry of the molecule but improves the quantitative agreement between calculated and measured angular distributions. The body-frame photoelectron angular distributions were measured in coincidence with the asymmetric $O^+ + CO^+$ ion fragmentation channel. In the mechanism for the combined photo- and Auger ionization process that we propose, the memory of the instantaneous position of the nuclei at the time of photoionization is imprinted on the final dication state, provided that the Auger decay occurs before vibrational motion *on the transient core-hole surface* can erase that memory. This means that the Auger decay time (~ 6 fs) must be less than or equal to half the asymmetric mode period, which is 7.2 fs, assuming that the asymmetric-stretch frequencies for the neutral and core-hole surfaces are comparable. We therefore incorporate the asymmetric-stretch motion of the neutral target into the observed MFPAD by confining the average to half of the allowed range of nuclear geometries, where one CO distance is elongated relative to the other. This treatment would be exact if the Auger decay was instantaneous. In fact, the transient core-hole state decays exponentially in time so that over half a vibrational period the true probability of decay is $\sim [1 - \exp(-7.2/6)] = 0.70$, which gives some indication of the extent to which our simple treatment may overestimate the observable asymmetry.

IV. RESULTS

The square-integrable portion of the basis for the complex Kohn calculations consisted of Dunning's double-zeta basis [11], augmented with two p-type, two d-type, and three f-type functions on the carbon atom, along with two p-type, two d-type, and one f-type function on the oxygen atoms. We also included numerical continuum functions up to $l=7$. To avoid working with nonorthogonal orbitals, we use a single set of molecular orbitals to construct both the initial neutral and final ion states, but two different procedures were used to generate these orbitals. In one case, we simply employed the occupied orbitals from an SCF calculation on neutral CO_2. In the second case, we start with a reference ion configuration with a single vacancy in the carbon $1s$ orbital. We then perform an all-singles configuration-interaction cal-
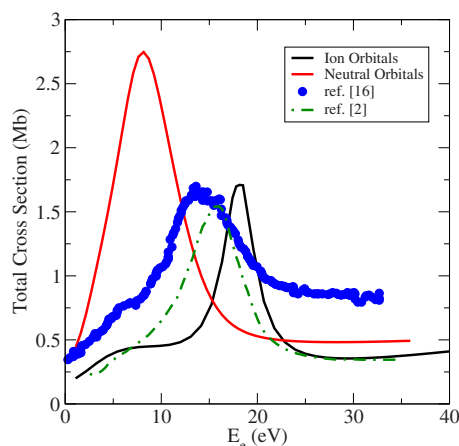
FIG. 3. (Color online) Total cross sections for $C(1s^{-1})$ photoionization. 1 Mb$=10^{-18}$ cm^2. Present results are compared with experimental yields of Bozek *et al.* [16] and theoretical calculations from Saito *et al.* [2].

culation, keeping the carbon $1s$ occupancy either one or zero. The natural orbitals from that calculation, obtained by diagonalizing the one-particle density matrix, are then used in the second set of photoionization calculations.

Figure 3 compares the total photoionization cross sections obtained with neutral and ion orbitals with the measured C $1s$ photoelectron yield [16] and the theoretical results reported by Saito *et al.* [2]. The experimental results were reported in arbitrary units, so they have been normalized to the results of our ion orbital calculation at the resonance maximum. The calculations done with ion orbitals are clearly in better agreement with experiment, giving a better value for the position of the $k\sigma_u$ shape resonance, as well as the shoulder near 6 eV photoelectron energy. Our ion orbital results are also in better agreement with the calculations by Saito *et al.* [2], which strike a balance between neutral and ion orbitals by using Slater's transition state approximation [17] to define a set of relaxed orbitals. The use of ion orbitals also results in a significant decrease in the magnitude of the cross section, reflecting the sensitivity of the underlying bound-free dipole matrix elements to the slight contraction of the carbon $1s$ orbital that results when it is singly occupied.

Figure 4 shows our calculated molecular-frame angular distributions for several photon energies for the case where the photon polarization lies along the molecular axis. These results are from calculations carried out with the nuclei fixed at the equilibrium geometry, and we again show results obtained with neutral and ion orbitals. The striking feature here is that the relatively simple two-lobed patterns seen at low and high photoelectron energies become highly structured over a rather narrow range of energies near 20 eV, where they show an almost complete extinction of probability for electron ejection along the molecular axis. This pattern is seen in calculations obtained with both neutral and ion orbitals, although the rapid changes are found at slightly lower energies in the neutral orbital calculations. Our ion orbital results are also found to be in excellent agreement with the theoretical MFPAD results reported by Liu *et al.* [3] (not shown).
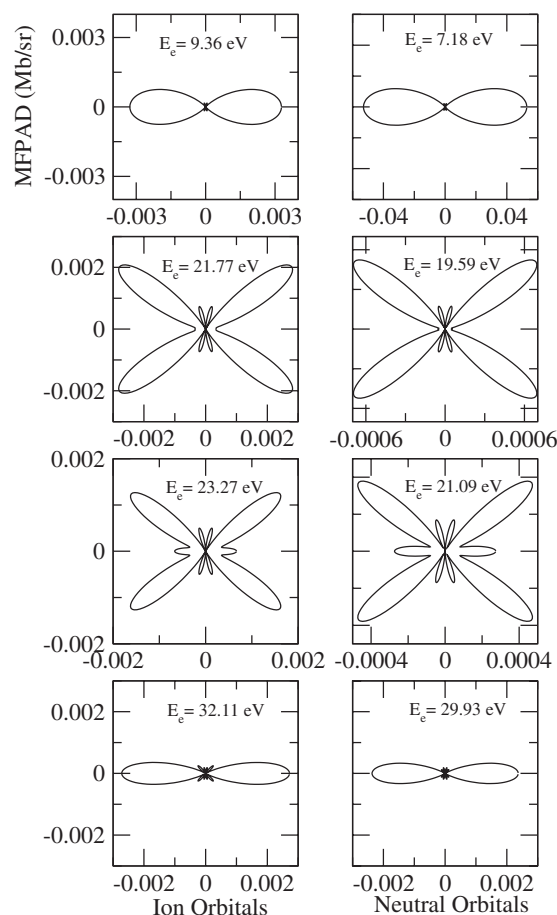

FIG. 4. Fixed-nuclei (equilibrium geometry) MFPAD in units of Mb/steradian, for polarization parallel to molecular axis.

The origin of the aforementioned pattern becomes clear when we examine the partial-wave contributions to the total cross section in Σ_u symmetry, which are shown in Fig. 5. It is seen that at photoelectron energies of 21.7 and 19.5 eV for the ion and neutral orbital calculations, respectively, the magnitudes of the $l=1$ and $l=5$ partial cross sections become equal. Moreover, at these energies, the $l=3$ partial cross sections are almost an order of magnitude smaller. These features are also evident in the calculations reported by Saito *et al.* [2] So the rapid change in the observed MFPADs is evidently the result of a destructive interference between the $l=1$ and $l=5$ amplitudes, which have the same magnitude at an energy where the $l=3$ contribution is small. We have confirmed this observation with calculations at other internuclear geometries, using both ion and neutral orbitals, finding that the sudden change in the MFPAD always appears at energies where the above conditions are met. We note in passing that the rapid changes in the observed angular distributions bear some resemblance to those seen in theoretical calculations on simple molecular targets which are produced by an effect that has been termed "partial-wave electron confinement" [18], although the underlying mechanisms are rather different.

Figure 6 shows molecular-frame angular distributions at four energies for the case of photon polarization perpendicular to the molecular axis. These results were calculated using
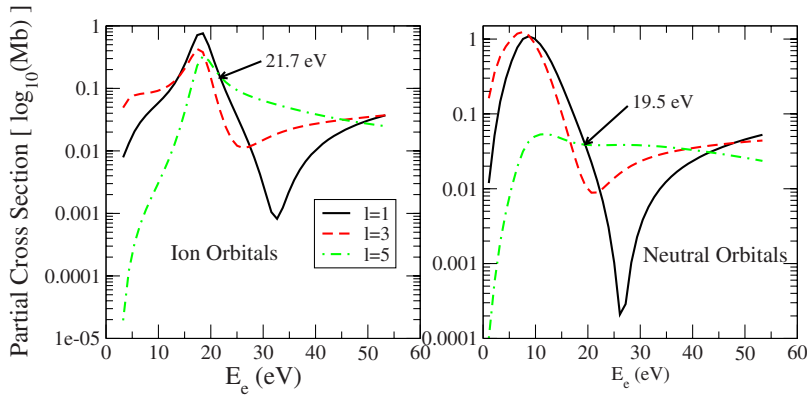
FIG. 5. (Color online) Σ_u partial-wave contributions to total cross sections for $C(1s^{-1})$ photoionization.

ion orbitals. Saito *et al.* [2] commented that at the lower photon energies the MFPAD exhibits a four-lobed structure characteristic of a d wave, which is forbidden in this channel. The observed structure is actually the result of interferences between the $l=1$ and $l=3$ partial-wave contributions. The magnitude of the $l=3$ contribution decreases as the energy increases, while the $l=1$ contribution remains relatively flat, producing a more characteristic p-wave-type structure as the energy increases. The structure seen at the highest energy reflects the increasing importance of the $l=5$ contribution.

To see the effect of asymmetric-stretch displacement of the nuclei from their equilibrium positions on the angular distributions, we show MFPADs in Σ symmetry in Fig. 7. The results shown were computed using ion orbitals with the nuclei at their root-mean-square (rms) displacements in the harmonic asymmetric-stretch potential and are plotted at the same energies shown in Fig. 4. The rms values were derived from a normal mode analysis of the ground-state CO_2 potential calculated at the MP2 level with a triple-zeta plus polarization basis. We remark that the rms values of the CO distances we used (2.146 and 2.254 bohr) differ from the values used by Liu *et al.* [3] (2.0773 and 2.3147). Asymmetry in the angular distributions is clearly evident in the calculated MF-

PADs. It is worth noting that the asymmetry effect is energy dependent. There is a shift in the asymmetry pattern as the energy passes through the region where the rapid changes in the MFPADs occur: below the "interference" region, ejection toward the CO^+ end of the asymmetrically stretched molecule is favored, while at higher energies, the probability of ejection shifts toward the O^+ side. Curiously, there is a reversal of this pattern as the photon energy is further increased, becoming symmetric near $E_e=49$ eV and favoring the CO^+ end at the highest energy. Indeed, the asymmetry shift appears to be correlated with the relative importance of the $l=1$ contribution (see Fig. 5), which may simply reflect the fact that this partial-wave penetrates the molecular core more than the higher $l=3,5,\ldots)$ components and may therefore be more sensitive to the fixed nuclear geometry.
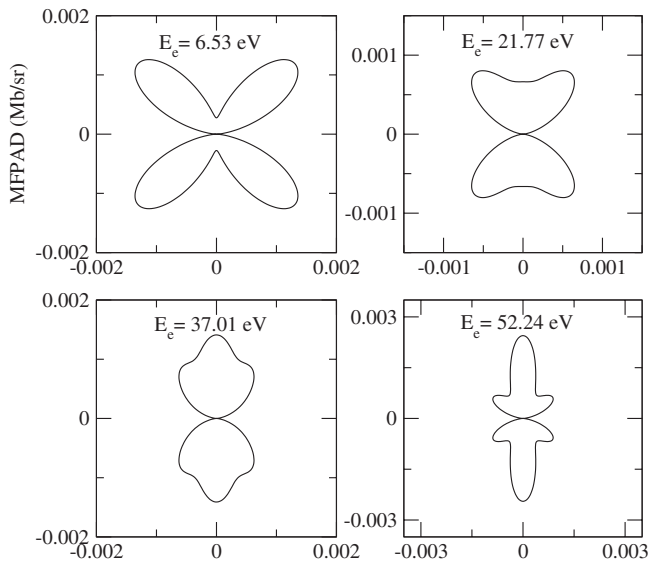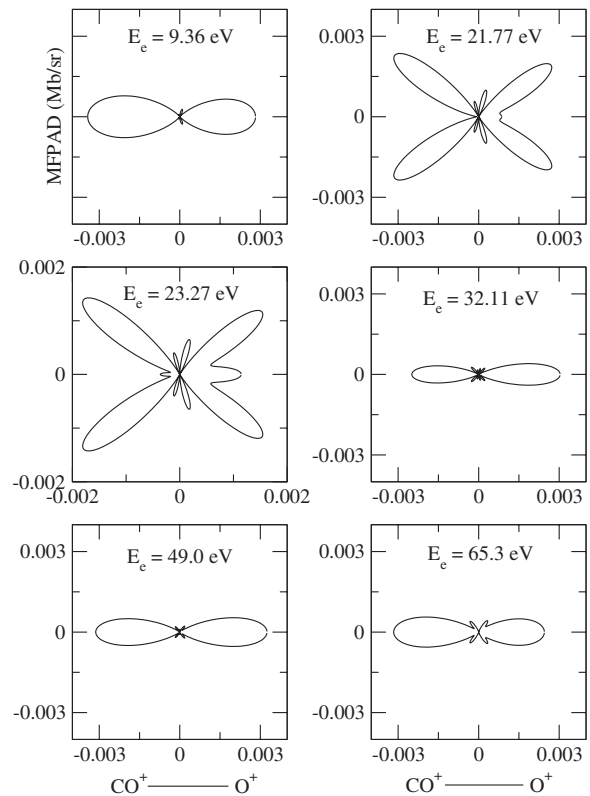

FIG. 7. As in Fig. 4 for asymmetric nuclear geometry. Calculations done using ion orbitals. CO distances are 2.146 and 2.254 bohr.

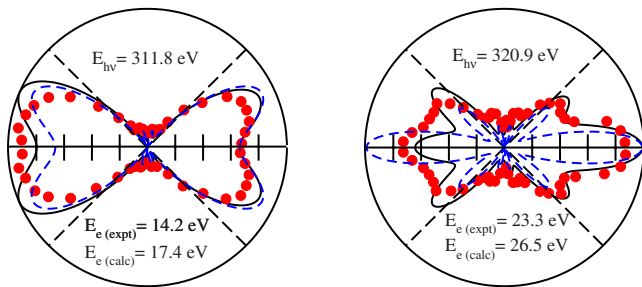FIG. 6. As in Fig. 4 for perpendicular polarization. Calculations done using ion orbitals.

FIG. 8. (Color online) Photoelectron angular distributions for $C(1s^{-1})$ ionization; photon polarization parallel to molecular axis. Solid curves: fixed-nuclei cross sections averaged over asymmetric-stretch and bending modes; broken curves: fixed-nuclei cross sections at equilibrium geometry. $E_{e(\text{expt})}$ and $E_{e(\text{calc})}$ refer to the experimental photoelectron energy and the energy used in the calculation, respectively (see text). Experimental points from Liu *et al.* [3]

For the comparison between measured and calculated MFPADs, we evaluated the differential photoionization cross section using Eq. (10), including the asymmetric-stretch and bending vibrational functions as outlined above. We have already noted that our ion orbital calculations place the Σ_u shape resonance ~ 3 eV higher than experiment [16]. To account for this difference when comparing theory with the experimental MFPADs of Lie *et al.* [3], we therefore subtracted 3 eV from the theoretical value of the photon energy associated with a particular photoelectron energy so that we are comparing cross sections measured at the same energy relative to the resonance peak. Figure 8 shows the results at two photon energies: one below and one above the "interference" region. The experimental photoelectron energies and the energies at which the calculations were performed are both indicated in the figure. We see that the shapes of the calculated and measured distributions, including the magnitudes of the asymmetry, are in good mutual agreement. (For comparison, the completely symmetric fixed-nuclei results calculated at the equilibrium geometry are also plotted.) Furthermore, the asymmetry shift from left to right is clearly seen in both the calculated and measured data.

V. DISCUSSION

We have carried out theoretical calculations of molecular-frame photoelectron angular distributions for $C(1s)$ ioniza-tion in CO_2 with a view toward explaining the weak but definite asymmetry seen when the photoelectons are measured in coincidence with asymmetric ion fragmentation. The asymmetry seen in the fixed-nuclei angular distributions with the nuclei displaced from their equilibrium positions by the root-mean-square values of the asymmetric-stretch normal coordinate is well correlated with the observed MFPADs. We have proposed a mechanism to explain how the memory of these photoelecton distributions produced from asymmetric geometries is imprinted on the nuclear dynamics following Auger decay. Since the Auger lifetime is shorter than the asymmetric-stretch vibrational period, population of an electronically excited dication state that produces $CO^+ + O^+$ fragment ions by direct dissociation can be used to monitor any asymmetry in the photoelectron angular distribution when measured in coincidence with the latter. Our electronic structure calculations on CO_2^{2+} have identified such a state. This mechanism explains how asymmetric angular distributions can be produced without invoking a breakdown of the two-step mechanism or the existence of an unlikely postcollision interaction between photo- and Auger electrons. We must emphasize that by the two-step model, we mean that the electronic photoelectron and Auger emission processes are independent. Photoelectron emission is, however, sensitive to nuclear geometry which varies over a slower time scale and provides the mechanism for imprinting any asymmetry in the instantaneous photoelectron angular distributions on the final ion fragmentation products. Finally, we believe that the fact that the shift in intensity of photoelectrons from CO^+ to O^+ as a function of photon energy is mirrored in the underlying fixed-nuclei MFPADs gives additional support to the proposed mechanism.

[1] E. Shigemasa, J. Adachi, M. Oura, and A. Yagishita, Phys. Rev. Lett. **74**, 359 (1995).

[2] N. Saito *et al.*, J. Phys. B **36**, L25 (2003).

[3] X.-J. Liu *et al.*, Phys. Rev. Lett. **101**, 083001 (2008).

[4] K. C. Prince, M. Avaldi, M. Coreno, R. Cammilloni, and M. de Simone, J. Phys. B **32**, 2551 (1999).

[5] M. Hochlaf, F. R. Bennett, G. Chambaud, and P. Rosmos, J. Phys. B **31**, 2163 (1998).

[6] T. X. Carroll, J. Hahne, T. D. Thomas, L. J. Saethre, N. Berrah, J. Bozek, and E. Kukk, Phys. Rev. A **61**, 042503 (2000).

[7] T. Kerkau and V. Schmidt, J. Phys. B **34**, 839 (2001).

[8] R. Püttner *et al.*, J. Phys. B **41**, 1 (2008).

[9] V. Feyer *et al.*, J. Chem. Phys. **123**, 224306 (2005).

[10] H. Ägren, J. Chem. Phys. **75**, 1267 (1981).

[11] T. Dunning, J. Chem. Phys. **53**, 2823 (1970).

[12] T. N. Rescigno, B. H. Lengsfield, and C. W. McCurdy, in *Modern Electronic Structure Theory*, edited by D. R. Yarkony (World Scientific, Singapore, 1995), Vol. 1.

[13] T. N. Rescigno, B. H. Lengsfield III, and A. E. Orel, J. Chem. Phys. **99**, 5097 (1993).

[14] T. N. Rescigno and A. E. Orel, Phys. Rev. A **43**, 1625 (1991).

[15] N. A. Cherepkov *et al.*, J. Phys. B **33**, 4213 (2000).

[16] J. D. Bozek, N. Saito, and I. H. Suzuki, Phys. Rev. A **51**, 4563 (1995).

[17] J. C. Slater, *The Self-Consistent Field for Molecules and Solids: Quantum Theory of Molecules and Solids* (McGraw-Hill, New York, 1974), Vol.4.

[18] J. Fernández, O. Fojón, A. Palacios, and F. Martín, Phys. Rev. Lett. **98**, 043005 (2007).